

Gradient-Based Predictive Pulse Pattern Control with Single-Phase Formulation

Ilari Hilden

Faculty of Inf. Technol. and Commun. Sciences
Tampere University
Tampere, Finland
ilari.hilden@tuni.fi

Petros Karamanakos

Faculty of Inf. Technol. and Commun. Sciences
Tampere University
Tampere, Finland
p.karamanakos@ieee.org

Tobias Geyer

Motion System Drives
ABB Switzerland Ltd
Turgi, Switzerland
t.geyer@ieee.org

Abstract—This paper presents a direct model predictive control (MPC) algorithm for three-phase power electronic systems, such as medium-voltage (MV) drives. The proposed control strategy manipulates a baseline pulse pattern, such as an optimized pulse pattern (OPP), in real time at the single-phase level, enabling independent control of the three phases. By doing so, this approach ensures excellent steady-state performance—quantified by the load current total demand distortion (TDD)—along with very short settling times during transients and excellent disturbance rejection. Additionally, by leveraging single-phase gradient based predictions, the proposed control strategy can tackle complex power electronic systems and demanding control problems with multiple—and possibly conflicting—control objectives. To highlight the superior performance of the proposed control strategy, comparisons with both conventional and advanced control methods are presented based on a case study involving a three-level neutral-point-clamped (NPC) inverter and an MV induction machine.

Index Terms—Model predictive control (MPC), optimized pulse patterns (OPPs), medium-voltage (MV) drives

I. INTRODUCTION

Power electronic systems are often nonlinear multiple-input multiple-output (MIMO) systems with actuators that operate in an on/off mode. Conventionally, pulse width modulation (PWM) such as carrier-based PWM (CB-PWM) or space vector modulation (SVM) is employed to conceal the switching nature on the system [1]. This simplifies the controller design and facilitates the use of (cascaded) single-input single-output (SISO) linear controllers. The separate computational stages of control and modulation, however, tend to limit the bandwidth of the controller [2]. Moreover, the different control loops are often insufficiently decoupled during transients, leading to adverse interactions. This implies that the bandwidth of the controller should be reduced further to avoid stability issues. Additionally, since linear controllers are typically tuned to achieve satisfactory performance only within a narrow operating range, their performance can degrade when operating outside of it. To address this, gain scheduling is often employed, which further complicates the tuning of the control loops and renders the whole design procedure cumbersome.

To overcome the limitations of linear control schemes, model predictive control (MPC) [3] has gained attention in the field of power electronics [4]. Particularly, MPC as a direct controller—i.e., where control and modulation are combined in

one computational stage—has been especially attractive due to its excellent dynamic performance and ability to handle nonlinear dynamics and MIMO systems [5]. The most widely adopted form of direct MPC, however—finite control set MPC (FCS-MPC)—leads to a variable switching frequency, which causes uneven stress among the semiconductor devices. Moreover, its steady-state performance can be inferior to linear control methods with a modulation stage. These drawbacks become particularly pronounced when operation at low switching frequencies is required, such as in the case of medium-voltage (MV) drives. Moreover, the lack of a periodic switching pattern results in nondeterministic harmonic spectra. This poses challenges when grid-connected operation is considered as strict grid codes, such as IEEE 519 [6], have to be met.

To address this problem, optimized pulse patterns (OPPs) can be utilized as they produce the minimum harmonic current distortions at a given switching frequency [7], [8]. To achieve fast closed-loop control with OPPs, MPC was employed in [9]. Owing to the OPPs, this method—referred to as model predictive pulse pattern control (MP³C)—can produce very low current distortions, while the direct manipulation of the OPPs allows for fast transients. To increase the versatility of MPC with OPPs, the so-called gradient-based predictive pulse pattern control (GP³C) was introduced in [10], and its performance was demonstrated in [11]. Even though this method manipulates OPPs in real time to achieve excellent output reference tracking, it is limited to a predefined set of switch positions, i.e., voltage vectors, dictated by the baseline pattern in use, i.e., the offline-computed OPP. This significantly reduces the degrees of freedom of the controller, thus limiting its bandwidth potential, robustness, and ability to reject disturbances effectively.

To overcome these limitations, this paper modifies GP³C from [10] to increase its degrees of freedom. Specifically, the switching time instants are optimized at the *single-phase* level—rather than the three-phase level as in [10]—by considering the contribution of each single-phase input to the gradient of the controlled variables. However, even though single-phase based optimization is utilized, full information of the three-phase system is retained. As a result, the proposed algorithm—hereafter referred to as S-GP³C—achieves excellent steady-state performance thanks to the baseline OPP.

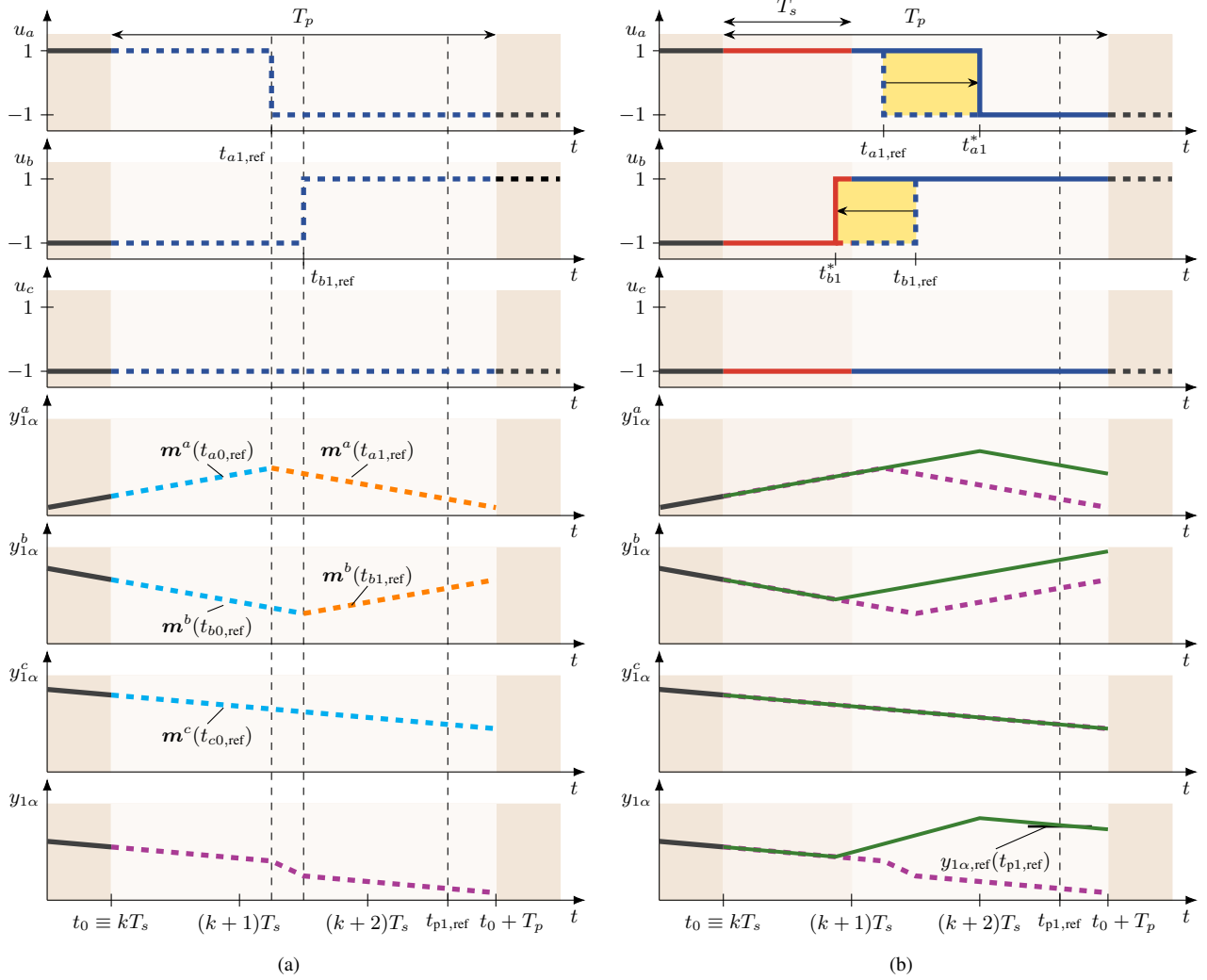


Fig. 2. Example of the gradient-based output evolution for a two-level converter within T_p when two reference time instants $t_{a1,ref}$ and $t_{b1,ref}$, and a single pivotal time instant $t_{p1,ref}$ are considered. The top three figures depict the three-phase pulse pattern, while figures 4–6 from the top show the evolution of the α -component of a single output variable y_1 based on the single-phase contribution of the gradients. The bottom figure shows the evolution of the complete component $y_{1\alpha}$. (a) Nominal (to-be-modified) pulse pattern and the gradients computed based on the nominal switching time instants. (b) The computed optimal modifications (indicated with arrows). The dash-dotted magenta lines show the evolution when the nominal pulse pattern is applied, while the green lines depict the evolution with the optimally modified pulse pattern. The black horizontal line shows the output reference $y_{1\alpha,ref}$ sampled at the pivotal time instant $t_{p1,ref}$.

ample, in Fig. 1, six subintervals are identified, i.e.,

$$\begin{aligned} & [t_0, t_{x1,ref}), [t_{x1,ref}, t_{x2,ref}), [t_{x2,ref}, t_{p1,ref}), \\ & [t_{p1,ref}, t_{x3,ref}), [t_{x3,ref}, t_{p2,ref}), [t_{p2,ref}, T_p). \end{aligned}$$

Therefore, to achieve accurate predictions, model (1) is discretized within each time interval $\Delta \tilde{t}_{x\ell,ref}$, resulting in the discrete-time state-space model

$$\mathbf{x}(\tilde{t}_{x\ell+1,ref}) = \mathbf{A}\mathbf{x}(\tilde{t}_{x\ell,ref}) + \mathbf{B}\mathbf{u}_{abc}(\tilde{t}_{x\ell,ref}) \quad (5a)$$

$$\mathbf{y}(\tilde{t}_{x\ell,ref}) = \mathbf{C}\mathbf{x}(\tilde{t}_{x\ell,ref}), \quad (5b)$$

with $\mathbf{A} = \mathbf{e}^{\mathbf{F}\Delta \tilde{t}_{x\ell,ref}}$ and $\mathbf{B} = -\mathbf{F}^{-1}(\mathbf{I} - \mathbf{A})\mathbf{G}$, where \mathbf{e} is the matrix exponential, and \mathbf{I} the identity matrix.

To analyze and predict the impact of a phase- x switch position on the dynamics of the system, its contribution is isolated. To this end, the “pseudo” three-phase switch positions \mathbf{u}_{abc}^x are introduced. These represent the effect of a phase

x while the other phases are assumed to be inactive. This decoupled representation simplifies the analysis by focusing on the unique influence of phase x on the system dynamics, independently of the combined three-phase behavior. The pseudo three-phase switch positions are defined as

$$\mathbf{u}_{abc}^a = \begin{bmatrix} u_a \\ 0 \\ 0 \end{bmatrix}, \mathbf{u}_{abc}^b = \begin{bmatrix} 0 \\ u_b \\ 0 \end{bmatrix}, \mathbf{u}_{abc}^c = \begin{bmatrix} 0 \\ 0 \\ u_c \end{bmatrix}, \quad (6)$$

such that $\mathbf{u}_{abc} = \mathbf{u}_{abc}^a + \mathbf{u}_{abc}^b + \mathbf{u}_{abc}^c$. Therefore, with the pseudo switch positions, the effect of u_x on the system dynamics can be computed at the nominal switching time instants $\tilde{t}_{x\ell,ref}$ in an iterative manner with (5), i.e.,

$$\mathbf{x}^x(\tilde{t}_{x\ell+1,ref}) = \mathbf{A}\mathbf{x}^x(\tilde{t}_{x\ell,ref}) + \mathbf{B}\mathbf{K}\mathbf{u}_{abc}^x(\tilde{t}_{x\ell,ref}) \quad (7a)$$

$$\mathbf{y}^x(\tilde{t}_{x\ell,ref}) = \mathbf{C}(\tilde{t}_{x\ell,ref}), \quad (7b)$$

where the initial state $\mathbf{x}^x(\tilde{t}_{x0,ref})$ is defined as

$\mathbf{x}^x(\tilde{t}_{x0,\text{ref}}) = \widetilde{\mathbf{K}}\mathbf{x}_{abc}^x(\tilde{t}_{x0,\text{ref}})$, with

$$\widetilde{\mathbf{K}} = \begin{bmatrix} \mathbf{K} & \mathbf{0}_{2 \times 3} & \cdots & \mathbf{0}_{2 \times 3} \\ \mathbf{0}_{2 \times 3} & \mathbf{K} & \cdots & \mathbf{0}_{2 \times 3} \\ \vdots & \vdots & \ddots & \vdots \\ \mathbf{0}_{2 \times 3} & \mathbf{0}_{2 \times 3} & \cdots & \mathbf{K} \end{bmatrix} \in \mathbb{R}^{n_x \times \frac{3n_x}{2}},$$

where \mathbf{K} is the transformation matrix

$$\mathbf{K} = \frac{2}{3} \begin{bmatrix} 1 & -\frac{1}{2} & -\frac{1}{2} \\ 0 & \frac{\sqrt{3}}{2} & -\frac{\sqrt{3}}{2} \end{bmatrix},$$

and $\mathbf{x}_{abc}^x \in \mathbb{R}^{\frac{3n_x}{2}}$ being the ‘‘pseudo-state’’ which isolates the state in phase x , i.e., it holds that

$$\mathbf{x}_{abc} = \widetilde{\mathbf{K}}^{-1}\mathbf{x} = \mathbf{x}_{abc}^a + \mathbf{x}_{abc}^b + \mathbf{x}_{abc}^c. \quad (8)$$

With the knowledge of phase- x contribution to the output of the system at time instants $\tilde{t}_{x\ell+1,\text{ref}}$ for $\ell \in \{0, 1, \dots, \tilde{z}_x\}$, i.e., $\mathbf{y}^x(\tilde{t}_{x0,\text{ref}}), \mathbf{y}^x(\tilde{t}_{x1,\text{ref}}), \dots, \mathbf{y}^x(\tilde{t}_{x\tilde{z}_x+1,\text{ref}})$, the evolution of the contribution within the intervals $\Delta\tilde{t}_{x\ell,\text{ref}}$ can be described by their corresponding gradients

$$\mathbf{m}^x(\tilde{t}_{x\ell,\text{ref}}) = \frac{\mathbf{y}^x(\tilde{t}_{x\ell+1,\text{ref}}) - \mathbf{y}^x(\tilde{t}_{x\ell,\text{ref}})}{\Delta\tilde{t}_{x\ell,\text{ref}}}. \quad (9)$$

Example 2. Consider the switching pattern within the prediction horizon T_p as shown in Fig. 2(a). Within the prediction horizon, there exists one nominal switching time instant in phases a and b , $t_{a1,\text{ref}}$ and $t_{b1,\text{ref}}$, respectively. Additionally, a pivotal time instant $t_{p1,\text{ref}}$, common for all three phases, is present. Therefore, the prediction horizon is divided into three subintervals in phases a and b , and into two in phase c . Within each of these subintervals the contribution of phase x to the output \mathbf{y}^x is assumed to evolve with a constant gradient. However, note that the gradients do not change at the pivotal time instant $t_{p1,\text{ref}}$, since the three-phase switch position \mathbf{u}_{abc} is kept constant. For clarity, only the α -component of a single output variable \mathbf{y}_1 is shown. Taking phase a as an example, to compute this evolution, described by the associated gradients, the interval $[t_{a0,\text{ref}}, t_{a1,\text{ref}}]$ is considered first.

Firstly, the continuous-time state space-space representation (1) is discretized with the sampling interval $\Delta t_{a0,\text{ref}} = t_{a1,\text{ref}} - t_{a0,\text{ref}}$ resulting in the discrete-time equivalent (5). With the initial state $\mathbf{x}^a(t_{a0,\text{ref}}) = \widetilde{\mathbf{K}}\mathbf{x}_{abc}^a(t_{a0,\text{ref}})$, the phase- a contribution to the state—and thus, the output—is computed at the end of the subinterval yielding $\mathbf{x}^a(t_{a1,\text{ref}})$. Subsequently, the gradient $\mathbf{m}^a(t_{a0,\text{ref}})$ is computed based on (9). The same procedure is then applied for the subsequent subintervals and repeated for phases b and c .

With the gradients $\mathbf{m}^x(\tilde{t}_{x\ell,\text{ref}})$, the system output at the to-be-computed modified time instants $t_{x\ell}$ can be derived. To this end, the vectors of the modified switching time instants \mathbf{t}_x and pivotal time instants \mathbf{t}_p are defined as

$$\mathbf{t}_x = [t_{x1} \ t_{x2} \ \cdots \ t_{xz_x}]^T \in \mathbb{R}^{z_x} \quad (10a)$$

$$\mathbf{t}_p = [t_{p1} \ t_{p2} \ \cdots \ t_{pz_p}]^T \in \mathbb{R}^{z_p}. \quad (10b)$$

Combining these vectors results in the vector of all the modified switching time instants $\tilde{\mathbf{t}}_x \in \mathbb{R}^{z_x}$ (see Example 1). The gradient-based predictions are explained with the following example.

Example 3. Consider again the example in Fig. 2(a). The prediction horizon is divided into three subintervals in phases a and b , and into two in phase c . Therefore, three gradients are computed in phases a and b , namely, $\mathbf{m}^a(\tilde{t}_{a0,\text{ref}}) \equiv \mathbf{m}^a(t_{a0,\text{ref}})$, $\mathbf{m}^a(\tilde{t}_{a1,\text{ref}}) \equiv \mathbf{m}^a(t_{a1,\text{ref}})$, and $\mathbf{m}^a(\tilde{t}_{a2,\text{ref}}) \equiv \mathbf{m}^a(t_{p1,\text{ref}})$ in phase a , while $\mathbf{m}^b(\tilde{t}_{b0,\text{ref}}) \equiv \mathbf{m}^b(t_{b0,\text{ref}})$, $\mathbf{m}^b(\tilde{t}_{b1,\text{ref}}) \equiv \mathbf{m}^b(t_{b1,\text{ref}})$, and $\mathbf{m}^b(\tilde{t}_{b2,\text{ref}}) \equiv \mathbf{m}^b(t_{p1,\text{ref}})$ are the gradients in phase b . Moreover, there are two gradients in phase c , i.e., $\mathbf{m}^c(\tilde{t}_{c0,\text{ref}}) \equiv \mathbf{m}^c(t_{c0,\text{ref}})$ and $\mathbf{m}^c(\tilde{t}_{c1,\text{ref}}) \equiv \mathbf{m}^c(t_{p1,\text{ref}})$. To compute the total output \mathbf{y} at the modified pivotal time instant t_{p1} , the contributions of each phase $\mathbf{y}^a(t_{p1})$, $\mathbf{y}^b(t_{p1})$, $\mathbf{y}^c(t_{p1})$, i.e.,

$$\begin{aligned} \mathbf{y}^a(t_{p1}) &= \mathbf{y}^a(t_{a0,\text{ref}}) + \mathbf{m}^a(t_{a0,\text{ref}})t_{a1} + \mathbf{m}^a(t_{a1,\text{ref}})(t_{p1} - t_{a1}) \\ \mathbf{y}^b(t_{p1}) &= \mathbf{y}^b(t_{b0,\text{ref}}) + \mathbf{m}^b(t_{b0,\text{ref}})t_{b1} + \mathbf{m}^b(t_{b1,\text{ref}})(t_{p1} - t_{b1}) \\ \mathbf{y}^c(t_{p1}) &= \mathbf{y}^c(t_{c0,\text{ref}}) + \mathbf{m}^c(t_{c0,\text{ref}})t_{p1}, \end{aligned}$$

are summed together where $t_{a0,\text{ref}} \equiv t_{b0,\text{ref}} \equiv t_{c0,\text{ref}} \equiv t_0 = 0$. This gives the closed-form expression

$$\begin{aligned} \mathbf{y}(t_{p1}) &= \mathbf{y}^a(t_{p1}) + \mathbf{y}^b(t_{p1}) + \mathbf{y}^c(t_{p1}) \\ &= \mathbf{y}(t_0) + (\mathbf{m}^a(t_{a0,\text{ref}}) - \mathbf{m}^a(t_{a1,\text{ref}}))t_{a1} + \\ &\quad + (\mathbf{m}^b(t_{b0,\text{ref}}) - \mathbf{m}^b(t_{b1,\text{ref}}))t_{b1} + \\ &\quad + (\mathbf{m}^a(t_{a1,\text{ref}}) + \mathbf{m}^b(t_{b1,\text{ref}}) + \mathbf{m}^c(t_{c0,\text{ref}}))t_{p1}. \end{aligned} \quad (12)$$

As explained in [10], objective function (4) can be approximated by evaluating the tracking error at specific discrete time instants. While this approximation is somewhat coarse, it provides sufficient accuracy to account for the rms value of the tracking error. Consequently, the desired system performance can be quantified using an objective function of the form

$$J = \sum_{j=1}^{z_p} \|\mathbf{y}_{\text{ref}}(t_{pj,\text{ref}}) - \mathbf{y}(t_{pj})\|_Q^2 + \lambda_t \|\Delta\mathbf{t}\|_2^2. \quad (13)$$

Note that the second term in (13) is defined as $\Delta\mathbf{t} = \mathbf{t}_{\text{ref}} - \mathbf{t}$, and it is added to penalize the deviations of the to-be-computed switching time instants \mathbf{t} from their nominal values \mathbf{t}_{ref} , where

$$\mathbf{t} = [\mathbf{t}_a^T \ \mathbf{t}_b^T \ \mathbf{t}_c^T \ \mathbf{t}_p^T]^T \in \mathbb{R}^{z_a+z_b+z_c+z_p} \quad (14a)$$

$$\mathbf{t}_{\text{ref}} = [\mathbf{t}_{a,\text{ref}}^T \ \mathbf{t}_{b,\text{ref}}^T \ \mathbf{t}_{c,\text{ref}}^T \ \mathbf{t}_{p,\text{ref}}^T]^T \in \mathbb{R}^{z_a+z_b+z_c+z_p}. \quad (14b)$$

Finally, the tuning parameter $\lambda_t \in \mathbb{R}^+$ sets the trade-off between the reference tracking accuracy and the control effort.

With some algebraic manipulations, the above objective function can be written in the compact vector form

$$J = \|\mathbf{r} - \mathbf{M}\mathbf{t}\|_Q^2 + \lambda_t \|\Delta\mathbf{t}\|_2^2, \quad (15)$$

where \mathbf{r} is a vector that depends on the reference values and the measurements of the output, \mathbf{M} is a matrix consisting of the gradients \mathbf{m}^x with which the output variables evolve within T_p , and $\mathbf{Q} = \text{diag}(Q, \dots, Q) \in \mathbb{R}^{n_y z_p \times n_y z_p}$ is a block

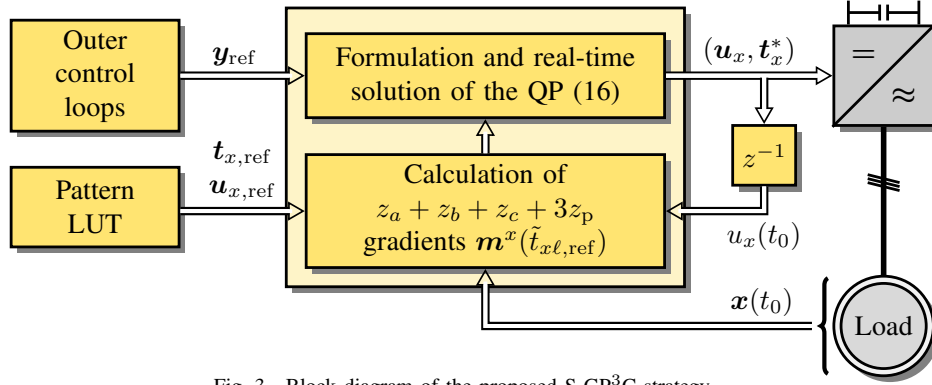


Fig. 3. Block diagram of the proposed S-GP³C strategy.

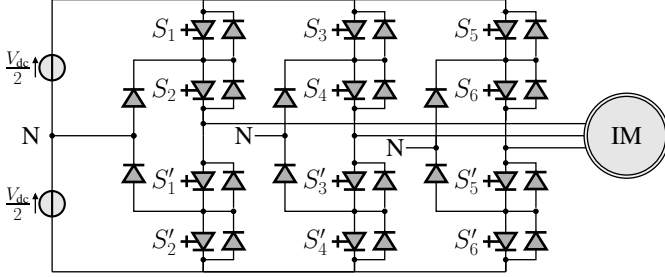


Fig. 4. A three-level NPC inverter driving an IM.

diagonal weighting matrix. The definitions of M and r are provided in Appendix A.

IV. CONTROL ALGORITHM

A step-by-step description of the proposed control algorithm is provided below, with an illustrative example shown in Fig. 2(b). The block diagram of the control strategy is presented in Fig. 3.

Step 1: In the first step, the nominal single-phase switching time instants $t_{x,\text{ref}}$, along with their corresponding single-phase switch positions u_x that fall within the prediction horizon T_p are obtained from a look-up-table (LUT). For simplicity, it can be assumed that these are based on an offline-computed OPP. Moreover, the nominal pivotal time instants $t_{p,\text{ref}}$ are inserted within the horizon. As a result, the comprehensive vector of total time instants $\tilde{t}_{x,\text{ref}}$, and the associated single-phase switch positions \tilde{u}_x for phase x are established. These vectors encapsulate all necessary time instants and their corresponding switch positions relevant to the prediction horizon T_p .

Step 2: With the knowledge of the \tilde{z}_x time instants $\tilde{t}_{x\kappa,\text{ref}}$, $\kappa \in \{1, 2, \dots, \tilde{z}_x\}$, and the corresponding $\tilde{z}_x + 1$ single-phase switch positions $\tilde{u}_x(\tilde{t}_{x\ell,\text{ref}})$, $\ell \in \{0, 1, \dots, \tilde{z}_x\}$, the gradients $m^x(\tilde{t}_{x\ell,\text{ref}})$ are computed with the help of (7) and (9). In total $z_a + z_b + z_c + 3z_p$ gradients need to be computed. Subsequently, the gradient matrix M and the reference vector r are formulated, see Appendix A.

Step 3: Following, the proposed MPC problem is formulated. To this end, objective function (15) is minimized by solving the following optimization problem, designed as a

TABLE I
RATED VALUES OF THE INDUCTION MACHINE

Parameter	Symbol	SI value
Voltage	V_R	3300 V
Current	I_R	356 A
Apparent power	S_R	2.034 MVA
Stator frequency	ω_{sR}	$2\pi 50$ rad/s
Rotational speed	ω_{mR}	596 rpm

TABLE II
SYSTEM PARAMETER VALUES IN THE P.U. SYSTEM

Parameter	Symbol	p.u.
Stator resistance	R_s	0.0108
Rotor resistance	R_r	0.0091
Stator leakage reactance	X_{ls}	0.1493
Rotor leakage reactance	X_{lr}	0.1104
Mutual reactance	X_m	2.3489
Dc-link voltage	V_{dc}	1.9299

quadratic program (QP)

$$\begin{aligned}
 & \underset{t}{\text{minimize}} && \|r - Mt\|_Q^2 + \lambda_t \|\Delta t\|_2^2 \\
 & \text{subject to} && t_0 \leq \tilde{t}_{a1} \leq \tilde{t}_{a2} \leq \dots \leq \tilde{t}_{a\tilde{z}_a} \leq t_0 + T_p \\
 & && t_0 \leq \tilde{t}_{b1} \leq \tilde{t}_{b2} \leq \dots \leq \tilde{t}_{b\tilde{z}_b} \leq t_0 + T_p \\
 & && t_0 \leq \tilde{t}_{c1} \leq \tilde{t}_{c2} \leq \dots \leq \tilde{t}_{c\tilde{z}_c} \leq t_0 + T_p.
 \end{aligned} \tag{16}$$

As can be seen, the to-be-computed switching and pivotal time instants must adhere to constraints that ensure their chronological order is preserved within each phase. However, unlike GP³C in [10], the switching time instants remain independent across the three phases within any given interval $[t_{pj}, t_{pj+1})$, enabling independent control at the single-phase level. This flexibility equips the controller with additional degrees of freedom, allowing it to introduce three-phase switch positions that do not exist in the baseline pattern. As a result, S-GP³C achieves superior overall performance, as demonstrated in Section V.

The QP (16) can be solved effectively using either standard off-the-shelf solvers or custom-designed in-house solvers

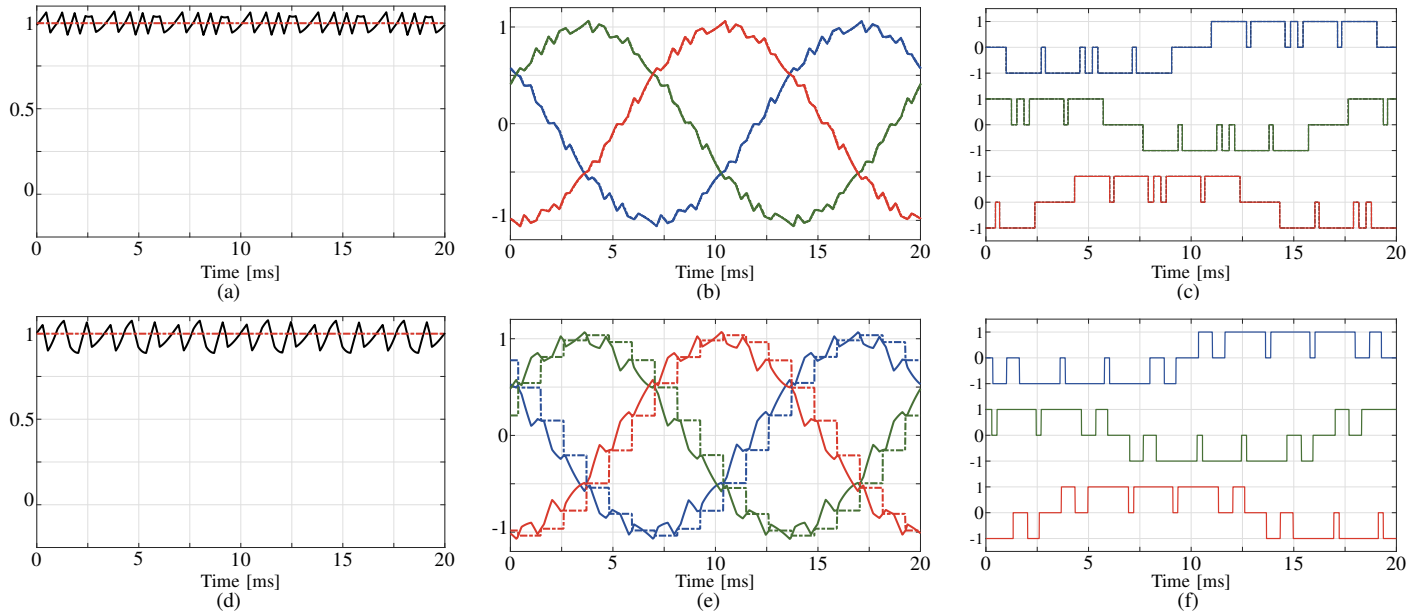


Fig. 5. Simulation results for (a)–(c) S-GP³C and (d)–(f) FOC with SVM during nominal operating conditions. (a), (d) Electromagnetic torque T_e (black line) and its reference (red dash-dotted line); (b), (e) three-phase stator currents $i_{s,abc}$ (solid lines) and their references (dash-dotted lines); (c) three-phase (modified) switching pattern (solid lines) and nominal OPP (dash-dotted lines); (f) three-phase switching pattern.

tailored for the specific problem. Solving this QP yields the vector of optimally modified *switching* and *pivotal* time instants, i.e.,

$$\mathbf{t}^* = \begin{bmatrix} \mathbf{t}_a^{*T} & \mathbf{t}_b^{*T} & \mathbf{t}_c^{*T} & \mathbf{t}_p^{*T} \end{bmatrix}^T, \quad (17)$$

where the \mathbf{t}_x^* and \mathbf{t}_p^* are the vectors of the optimally modified phase- x switching and pivotal time instant, respectively.

Step 4: In the final step of the control procedure, the optimal switching time instants \mathbf{t}^* that fall within the first sampling interval T_s of the prediction horizon T_p , i.e., the interval $[kT_s, (k+1)T_s)$, are applied to the converter. Following the receding horizon principle inherent to MPC, the prediction window is then shifted forward by one sampling interval T_s . The control algorithm is subsequently reinitialized, starting again from the first step, ensuring continuous system operation and feedback integration.

V. CASE STUDY

The proposed S-GP³C algorithm is implemented as current controller in a 2 MVA drive system consisting of a three-level neutral-point-clamped (NPC) inverter and an MV induction machine, as shown in Fig. 4. It is assumed that the dc-link voltage V_{dc} is constant and the NP potential fixed to zero. The rated values of the machine are provided in Table I while the drive parameters are shown in Table II. The drive model, including the continuous-time state-space model (1) matrices, is given in Appendix B. A three-level OPP is used as the baseline pulse pattern and it has a pulse number $d = 5$ resulting in a device switching frequency of 250 Hz at nominal speed. The modulation index is $m = 1.046$. As for the controller parameters, the sampling interval is set to $T_s = 50 \mu\text{s}$ and a prediction horizon of 25 time steps is used.

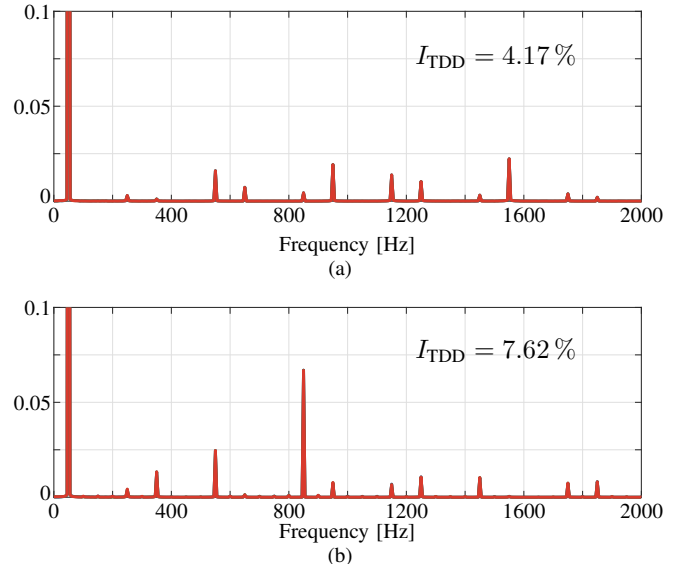


Fig. 6. Stator current frequency spectra at nominal operating conditions; (a) S-GP³C, (b) FOC with SVM.

The weighting factor λ_t is set to a value of $4 \cdot 10^6$. Finally, all results are shown in the per unit (p.u.) system.

The steady-state performance of the proposed S-GP³C strategy is examined at rated torque and nominal speed. The corresponding results are shown in Fig. 5. As can be seen, the stator current tracking performance of S-GP³C is excellent and only minute modifications to the nominal OPP are needed to correct the tracking error, thus ensuring that the electromagnetic torque accurately follows its reference. Moreover, the ability of S-GP³C to use an OPP as a baseline pulse pattern results in a very low stator current TDD of only 4.17%, despite the very low switching frequency. Furthermore, as can

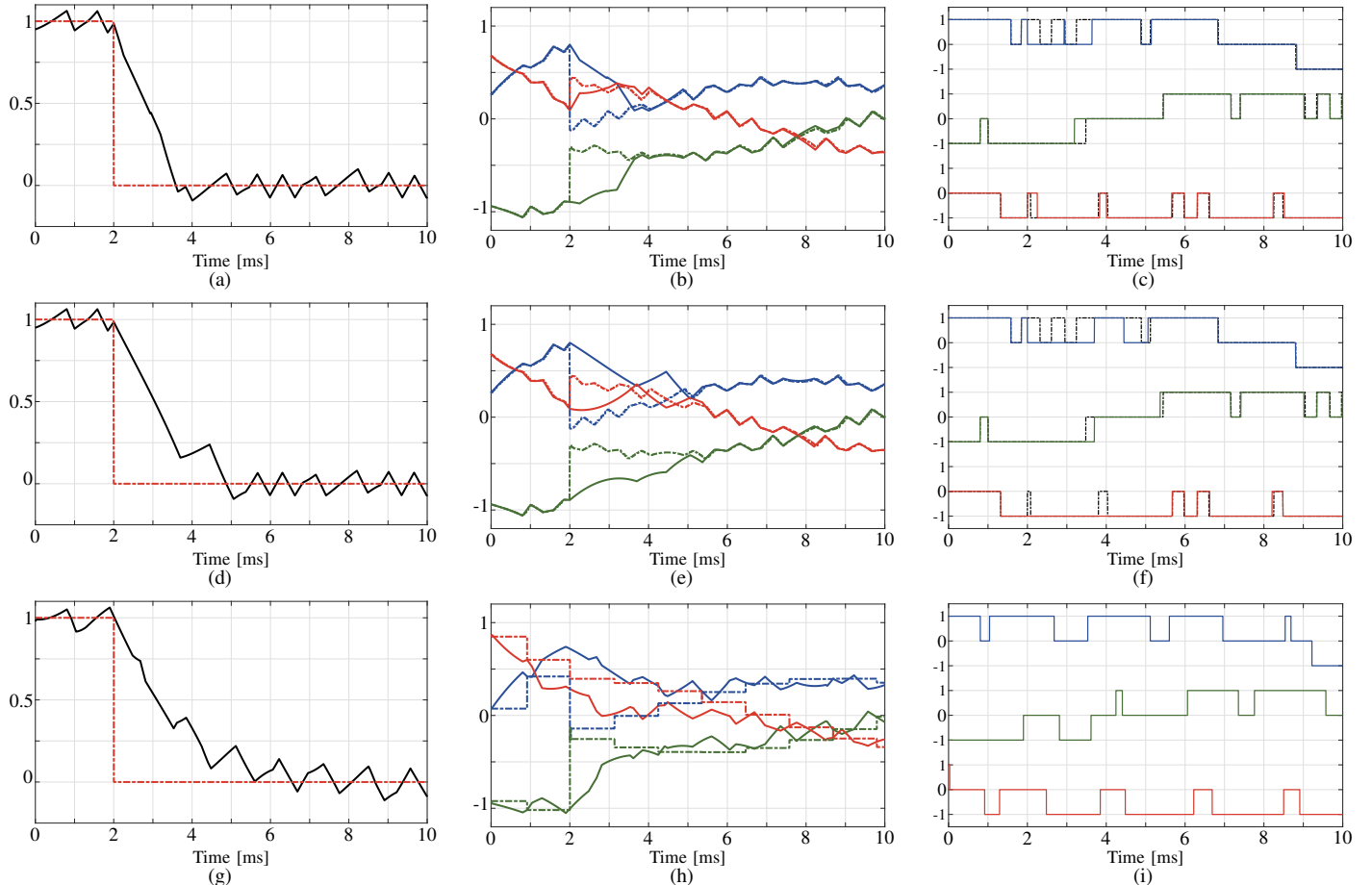


Fig. 7. Simulation results for a torque reference step down for: (a)–(c) S-GP³C; (d)–(e) GP³C; and (g)–(i) FOC with SVM. (a), (d), (g) Electromagnetic torque T_e (black line) and its reference (red dash-dotted line); (b), (e), (h) three-phase stator currents $\hat{i}_{s,abc}$ (solid lines) and their references (dash-dotted lines); (c), (f), (i) three-phase (modified) switching pattern (solid lines) and nominal OPP (dash-dotted lines).

be seen in Fig. 6(a), the current harmonics are located at the nontriplen odd multiples of the fundamental frequency thanks to the symmetry properties of the OPP, which are preserved by the controller to some extent. In contrast, field-oriented control (FOC) with SVM (see Figs. 5(d)–5(f)) operating at the same switching frequency, produces a stator current TDD of 7.62%, i.e., more than 80% higher than S-GP³C (see Fig. 6(b)).

The improved dynamic performance is demonstrated by comparing the proposed S-GP³C, with GP³C from [10] and FOC with SVM in Fig. 7. Therein, the torque is stepped down from 1 p.u. to 0 p.u. at $t = 2$ ms. As shown, S-GP³C achieves the fastest settling time—over 50% faster than the other methods—due to the optimization of the switching time instants at the single-phase level, allowing independent control of the three phases. This effect is evident in Fig. 7(c), where, e.g., at 2 ms the controller introduces the three-phase switch position $[0 \ -1 \ 0]$, which is not locally present in the OPP. This is something that GP³C from [10], by definition, cannot achieve (see Fig. 7(f)), as it controls all three phases simultaneously, which limits its dynamic response. It is important to note that while this capability allows for faster transients and better disturbance rejection, it also facilitates the control of complex systems, such as back-to-back configuration, with a single controller.

VI. CONCLUSION

This paper proposed a control strategy referred to as S-GP³C, which combines MPC with optimal modulation in the form of OPPs. The discussed approach is a derivative of GP³C, introduced in [10], with a fundamental difference that offers additional degrees of freedom. This is achieved by utilizing a single-phase contribution-based prediction model enabling individual manipulation of the switching time instants at the single-phase level. As a result, not only excellent steady-state performance is achieved—owing to the use of an OPP as a baseline pattern—but also faster transient responses, improved disturbance rejection, and greater design versatility. These features make S-GP³C particularly well-suited for systems with highly complex dynamics. The presented results demonstrate the superior performance of the proposed control scheme compared to both the conventional GP³C as well as established methods, such as FOC with SVM.

APPENDIX A DESCRIPTION OF THE OBJECTIVE FUNCTION

By generalizing the expression (12), it can be shown that the output at the modified pivotal time instants t_{pj} can be written

in the vector form

$$\begin{bmatrix} \mathbf{y}(t_{p1}) \\ \mathbf{y}(t_{p2}) \\ \vdots \\ \mathbf{y}(t_{pz_p}) \end{bmatrix} = \begin{bmatrix} \mathbf{y}(t_0) \\ \mathbf{y}(t_0) \\ \vdots \\ \mathbf{y}(t_0) \end{bmatrix} + \begin{bmatrix} \mathbf{M}_a & \mathbf{M}_b & \mathbf{M}_c & \mathbf{M}_p \end{bmatrix} \mathbf{t},$$

where matrix $\mathbf{M}_x \in \mathbb{R}^{n_y z_p \times z_x}$, $x \in \{a, b, c\}$, is given by

$$\mathbf{M}_x = \begin{bmatrix} \mathbf{m}_0^x & \mathbf{m}_1^x & \cdots & \mathbf{m}_{z_{x1}}^x & \mathbf{0}_{n_y \times 1} & \mathbf{0}_{n_y \times 1} & \mathbf{0}_{n_y \times 1} & \cdots & \mathbf{0}_{n_y \times 1} \\ \mathbf{m}_0^x & \mathbf{m}_1^x & \cdots & \cdots & \cdots & \mathbf{m}_{z_{x1}+z_{x2}}^x & \mathbf{0}_{n_y \times 1} & \cdots & \mathbf{0}_{n_y \times 1} \\ \vdots & \vdots & \vdots & \vdots & \vdots & \vdots & \vdots & \ddots & \vdots \\ \mathbf{m}_0^x & \mathbf{m}_1^x & \cdots & \cdots & \cdots & \cdots & \cdots & \cdots & \mathbf{m}_{\sum_{j=1}^{z_p} z_{xj}}^x \end{bmatrix}$$

with $\mathbf{m}_j^x = \mathbf{m}^x(t_{xj,\text{ref}}) - \mathbf{m}^x(t_{xj+1,\text{ref}})$, and z_{xj} being the number of the nominal switching time instants between two consecutive pivotal time instants, i.e., it holds that $\sum_{j=1}^{z_p} z_{xj} = z_x$. Moreover, the matrix $\mathbf{M}_p \in \mathbb{R}^{n_y z_p \times z_p}$ is given by

$$\mathbf{M}_p = \begin{bmatrix} \overline{\mathbf{m}}_{p0} & \mathbf{0}_{n_y \times 1} & \cdots & \cdots & \mathbf{0}_{n_y \times 1} \\ \mathbf{m}_{p0} & \overline{\mathbf{m}}_{p1} & \cdots & \cdots & \mathbf{0}_{n_y \times 1} \\ \vdots & \vdots & \vdots & \ddots & \vdots \\ \mathbf{m}_{p0} & \mathbf{m}_{p1} & \cdots & \cdots & \overline{\mathbf{m}}_{pz_p} \end{bmatrix},$$

where

$$\overline{\mathbf{m}}_{pj} = \mathbf{m}^a(t_{az_{aj},\text{ref}}) + \mathbf{m}^b(t_{bz_{bj},\text{ref}}) + \mathbf{m}^c(t_{cz_{cj},\text{ref}}),$$

and

$$\mathbf{m}_{pj-1} = \mathbf{m}^a(t_{az_{aj},\text{ref}}) + \mathbf{m}^b(t_{bz_{bj},\text{ref}}) + \mathbf{m}^c(t_{cz_{cj},\text{ref}}) - (\mathbf{m}^a(t_{az_{aj}+1,\text{ref}}) + \mathbf{m}^b(t_{bz_{bj}+1,\text{ref}}) + \mathbf{m}^c(t_{cz_{cj}+1,\text{ref}})).$$

Based on the above, the vector \mathbf{r} and the matrix \mathbf{M} in (15) are given by

$$\mathbf{r} = \begin{bmatrix} \mathbf{y}_{\text{ref}}(t_{p1,\text{ref}}) - \mathbf{y}(t_0) \\ \mathbf{y}_{\text{ref}}(t_{p2,\text{ref}}) - \mathbf{y}(t_0) \\ \vdots \\ \mathbf{y}_{\text{ref}}(t_{pz_p,\text{ref}}) - \mathbf{y}(t_0) \end{bmatrix},$$

and

$$\mathbf{M} = \begin{bmatrix} \mathbf{M}_a & \mathbf{M}_b & \mathbf{M}_c & \mathbf{M}_p \end{bmatrix}.$$

APPENDIX B

MODEL OF THE MV DRIVE SYSTEM

The drive system in Section V is modeled in the stationary orthogonal ($\alpha\beta$) plane. The state consists of the stator current and rotor flux, i.e., $\mathbf{x} = [i_{s\alpha} \ i_{s\beta} \ \psi_{r\alpha} \ \psi_{r\beta}]^T \in \mathbb{R}^4$. The input is the three-phase switch position $\mathbf{u}_{abc} \in \{-1, 0, 1\}^3$, while the stator current serves as the system output, i.e., $\mathbf{y} = \mathbf{i}_s \in \mathbb{R}^2$. By modeling the dynamics of the MV drive system, a continuous-time state-space model of the form (1) is obtained,

where the matrices are defined as [12]

$$\mathbf{F} = \begin{bmatrix} -\frac{1}{\tau_s} & 0 & \frac{X_m}{\tau_r D} & \omega_r \frac{X_m}{D} \\ 0 & -\frac{1}{\tau_s} & -\omega_r \frac{X_m}{D} & \frac{X_m}{\tau_r D} \\ \frac{X_m}{\tau_r} & 0 & -\frac{1}{\tau_r} & -\omega_r \\ 0 & \frac{X_m}{\tau_r} & \omega_r & -\frac{1}{\tau_r} \end{bmatrix},$$

$$\mathbf{G} = \frac{V_{\text{dc}} X_r}{2 D} \begin{bmatrix} 1 & 0 \\ 0 & 1 \\ 0 & 0 \\ 0 & 0 \end{bmatrix} \mathbf{K}, \quad \mathbf{C} = \begin{bmatrix} 1 & 0 & 0 & 0 \\ 0 & 1 & 0 & 0 \end{bmatrix},$$

where $\tau_s = X_r D / (R_s X_r^2 + R_r X_m^2)$ and $\tau_r = X_r / R_r$, are the transient stator and rotor time constants, respectively, and $D = X_s X_r - X_m^2$, with $X_s = X_{ls} + X_m$ and $X_r = X_{lr} + X_m$, being the stator and rotor self reactances, respectively, while X_{ls} , X_{lr} , and X_m are the stator leakage, rotor leakage, and mutual reactances, respectively. Finally, R_s and R_r are the stator and rotor resistances, respectively, and ω_r is the rotor (electrical) speed.

ACKNOWLEDGMENTS

This work was supported by the Research Council of Finland.

REFERENCES

- [1] J. Holtz, "Pulsewidth modulation for electronic power conversion," *Proc. IEEE*, vol. 82, no. 8, pp. 1194–1214, Aug. 1994.
- [2] J. Rodríguez, R. M. Kennel, J. R. Espinoza, M. Trincado, C. A. Silva, and C. A. Rojas, "High-performance control strategies for electrical drives: An experimental assessment," *IEEE Trans. Ind. Electron.*, vol. 59, no. 2, pp. 812–820, Feb. 2012.
- [3] J. B. Rawlings and D. Q. Mayne, *Model Predictive Control: Theory and Design*. Madison, WI: Nob Hill, 2009.
- [4] S. Kouro, M. A. Perez, J. Rodríguez, A. M. Llor, and H. A. Young, "Model predictive control: MPC's role in the evolution of power electronics," *IEEE Ind. Electron. Mag.*, vol. 9, no. 4, pp. 8–21, Dec. 2015.
- [5] S. Vazquez, J. Rodríguez, M. Ricera, L. G. Franquelo, and M. Norambuena, "Model predictive control for power converters and drives: Advances and trends," *IEEE Trans. Ind. Electron.*, vol. 64, no. 2, pp. 935–947, Feb. 2017.
- [6] IEEE Std 519-2014 (Revision of IEEE Std 519-1992), "IEEE recommended practices and requirements for harmonic control in electrical power systems," pp. 1–29, Jun. 2014.
- [7] G. S. Buja and G. B. Indri, "Optimal pulsewidth modulation for feeding ac motors," *IEEE Trans. Ind. Appl.*, vol. IA-13, no. 1, pp. 38–44, Jan. 1977.
- [8] G. S. Buja, "Optimum output waveforms in PWM inverters," *IEEE Trans. Ind. Appl.*, vol. IA-16, no. 6, pp. 830–836, Nov./Dec. 1980.
- [9] T. Geyer, N. Oikonomou, G. Papafotiou, and F. D. Kieferndorf, "Model predictive pulse pattern control," *IEEE Trans. Ind. Appl.*, vol. 48, no. 2, pp. 663–676, Mar./Apr. 2012.
- [10] M. A. W. Begh, P. Karamanakos, and T. Geyer, "Gradient-based predictive pulse pattern control of medium-voltage drives—Part I: Control, concept, and analysis," *IEEE Trans. Power Electron.*, vol. 37, no. 12, pp. 14 222–14 236, Dec. 2022.
- [11] M. A. W. Begh, P. Karamanakos, T. Geyer, and Q. Yang, "Gradient-based predictive pulse pattern control of medium-voltage drives—Part II: Performance assessment," *IEEE Trans. Power Electron.*, vol. 37, no. 12, pp. 14 237–14 251, Dec. 2022.
- [12] J. Holtz, "The representation of ac machine dynamics by complex signal flow graphs," *IEEE Trans. Ind. Electron.*, vol. 42, no. 3, pp. 263–271, Jun. 1995.